processes

MDPI

Article

Experimental Investigation of Factors Influencing Spontaneous Imbibition in Shale Reservoirs

Li Liu [1], Yi-Min Wang [1,*], Ai-Wei Zheng [1], Ji-Qing Li [2], Qian Zhang [1], Ya-Wan Tang [1], Wen-Xin Yang [1], Mingjun Chen [3] and Shuqiang Shi [4]

[1] Exploration and Development Research Institute, Jianghan Oilfield Branch Company, Sinopec, Wuhan 430223, China
[2] Jianghan Oilfield Branch Company, Sinopec, Qianjiang 433124, China
[3] State Key Laboratory of Oil and Gas Reservoir Geology and Exploitation, Southwest Petroleum University, Chengdu 610500, China
[4] School of Petroleum Engineering, Chongqing University of Science & Technology, Chongqing 401331, China
* Correspondence: swpuwym@163.com

Abstract: The flowback rate of fracturing fluid in shale reservoirs is often notably low, primarily due to the spontaneous imbibition of the water-based fracturing fluid. Despite their significance, the factors influencing spontaneous imbibition in shale reservoirs remain insufficiently understood. Moreover, whether spontaneous imbibition is ultimately beneficial or detrimental to shale reservoirs is still a subject of debate. This study investigates the spontaneous imbibition process in shale, the factors (the bedding, contact area, porosity, initial water saturation, and fluid type) affecting it, and its impact on shale porosity and permeability. The results reveal that the spontaneous imbibition process can be categorized into three distinct stages: the rapid imbibition stage, the transitional stage, and the stable stage. It is observed that bedding significantly influences the imbibition rate, and the imbibition rate in the parallel bedding direction is greater than that in the vertical bedding direction. The imbibition capacity increases with larger contact area and higher porosity, while it decreases with higher initial water saturation. Furthermore, the imbibition capacity varies with the type of fluid, following this order: distilled water > 5% KCl solution > kerosene. The maximum imbibed volume per unit pore volume of shale in distilled water is twice that in kerosene. Lastly, spontaneous imbibition is found to enhance the porosity and permeability of shale. After three instances of imbibition, the porosity of the matrix and fractured sample increased by 0.85% and 1.68%, and the permeability increased by 0.636 mD and 0.829 mD, respectively.

Keywords: shale; spontaneous imbibition; imbibition capacity; imbibition rate

check for updates

Academic Editor: Qingbang Meng

Received: 14 December 2024
Revised: 29 January 2025
Accepted: 5 February 2025
Published: 11 February 2025

Citation: Liu, L.; Wang, Y.-M.; Zheng, A.-W.; Li, J.-Q.; Zhang, Q.; Tang, Y.-W.; Yang, W.-X.; Chen, M.; Shi, S. Experimental Investigation of Factors Influencing Spontaneous Imbibition in Shale Reservoirs. *Processes* **2025**, *13*, 503. https://doi.org/10.3390/pr13020503

Copyright: © 2025 by the authors. Licensee MDPI, Basel, Switzerland. This article is an open access article distributed under the terms and conditions of the Creative Commons Attribution (CC BY) license (https://creativecommons.org/licenses/by/4.0/).

1. Introduction

Shale reservoirs are a typical unconventional resource and represent a significant energy supply to meet increased global energy demands [1,2]. Despite their low porosity and ultralow matrix permeability, economic production is made possible through the injection of large volumes of water-based fracturing fluid. This process creates hydraulic fractures in the formations, which are kept open using proppants [3,4]. However, during hydraulic fracturing, less than 30%, and in some cases less than 10%, of the injected water-based fracturing fluid is recovered during the flowback stage [5,6].

The primary mechanism behind this low recovery is the spontaneous imbibition of water-based fracturing fluid into the shale matrix [7,8]. Additional mechanisms include

fluid retention due to fracture closure during early flowback [9,10] and gravity segregation effects [11,12].

Spontaneous imbibition is an immiscible displacement process in porous media, which is caused by differential absorption between the pore throat wall and the fluid. While it is the primary cause of clay damage in clay-rich shale formations and water blockage in tight gas reservoirs [13], it is governed by capillary pressure, which is related to wettability [14–16], interfacial tension [17] and pore radius [18]. Capillary forces can substantially enhance the imbibition of the injected water into the water-wet formations, while this effect is negligible in intermediate-wet formations [19].

The impact of spontaneous imbibition on shale reservoir productivity has been the subject of significant interest [20–24]. On the one hand, imbibition of water-based fracturing fluid can lead to fluid retention near the fracture surface due to strong capillary pressure, thereby reducing gas relative permeability and production [25–28]. Additionally, clay swelling and dispersion caused by imbibition may damage absolute permeability [29–31].

On the other hand, some scholars think that the spontaneous imbibition is beneficial to production due to the capillary pressure in water-wet facies [32] and permeability increases which are caused by the mineral dissolution and microfractures formation [33–35]. Consequently, it remains unclear whether spontaneous imbibition is ultimately detrimental or beneficial to shale reservoirs. Furthermore, the recent development of experimental methods focuses on the use of high-resolution measurement technology (nuclear magnetic resonance, CT scanning three-dimensional imaging technology) to monitor the imbibition process and reveal the mechanism of imbibition [36,37]. Limited research exists on the analysis of influencing factors of spontaneous imbibition for shale. Moreover, the experimental method of measuring sample mass [38] has a relative large measurement error.

In this study, an improved experimental method was used to investigate the process of spontaneous imbibition, as well as the effects of bedding, contact area, porosity, initial water saturation, and fluid type. Additionally, changes in the porosity and permeability of shale samples before and after imbibition were recorded and analyzed. The findings contribute to a better understanding of the imbibition process, its influencing factors, and its effects on shale porosity and permeability.

2. Spontaneous Imbibition Experiment

2.1. Experimental Samples

The samples used in this work for experiments were sourced from the Longmaxi Formation in the Jiaoshiba area in the eastern Sichuan Basin in China. The Sichuan Basin lies on the western margin of the Yangtze Platform. Tectonically, the Jiaoshiba area of the Fuling gas field is on the western side of the Qiyueshan fault, which marks the basin's boundary. The region's structure trends northeast, consistent with the nearby Huayingshan and Qiyueshan faults. The primary gas-bearing strata are organic-rich shales from the Wufeng (Late Ordovician) and Longmaxi (Early Silurian) Formations. The lower part of the Longmaxi shale is mainly dominated by black carbonaceous shale and siliceous shale, containing a large amount of radiolarian, calthrop and graptolite fossils.

In this work, the target depth is between 2309 and 2609 m, the target temperature is averaged to be 82 °C, and the target pressure is averaged to be 37.7 MPa. The average natural gas content in the shale gas reservoir is 98.27%, and the relative density is 0.5656 g/cm^3. The initial water saturation is 15.5–48.6% based on well logging. The TOC is 0.55–5.89%, and the Ro is 2.2–3.06%. Photos of a full-diameter shale core and wax-sealed sample before testing are shown in Figures 1a and 1b, respectively. A total of 22 samples were collected from the Longmaxi Formation in the Jiaoshiba area. In the preparation stage,

the permeability and porosity of the 22 samples were measured and the measured results are shown in Table 1. In addition, the sides of samples were all wax-sealed.

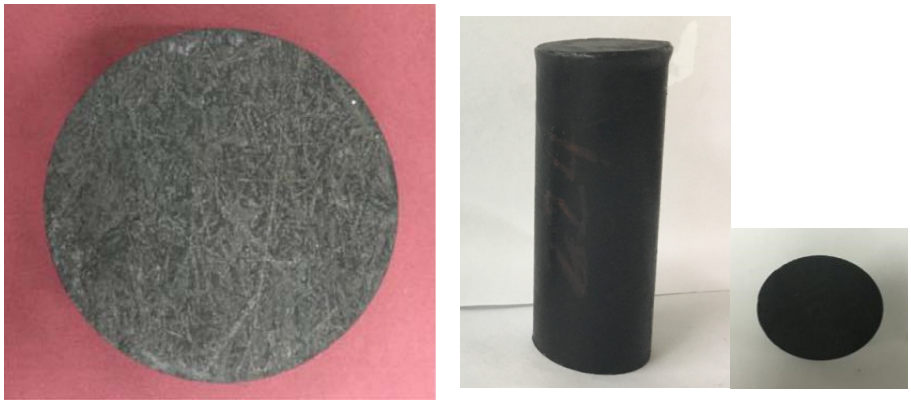

(**a**) (**b**)

Figure 1. Photos of Longmaxi shale samples in this work: (**a**) a full-diameter core; (**b**) a wax-sealed sample before testing.

Table 1. The physical parameters of 22 samples.

Sample Number	Length (mm)	Diameter/Area (mm)/(cm^2)	Porosity (%)	Permeability (mD)
1	50	25	4.34	0.96091
2	50	25	3.80	0.23449
3	50	25	3.68	0.01581
4	50	25	3.11	0.00801
5	50	25	2.51	0.00402
6	50	25	2.86	0.10843
7	50	25	2.13	0.00356
8	50	25	2.32	0.00452
9	50	8.20 (area)	2.33	0.03271
10	50	5.77 (area)	2.93	0.03953
11	50	4.84 (area)	2.74	0.03597
12	50	25	3.74	0.04253
13	50	25	4.51	0.04397
14	50	25	2.06	0.04017
15	50	25	2.92	1.16313
16	50	25	2.56	1.18321
17	50	25	2.60	1.35217
18	50	25	4.10	0.04171
19	50	25	4.30	0.04244
20	50	25	3.97	0.03743
21	81	25	1.12	0.02112
22	81	25	3.01	0.08300

2.2. Experimental Method and Test Procedure

The spontaneous imbibition experiments in this study were conducted using the mass measurement method (see Figure 2). The beaker used in the experiment is 250 mL, and the weighing experimental apparatus used is the JJBC series electronic analytical balance, as shown in Figure 2b. The accuracy of the apparatus is 0.1 mg, and the volume is 220(W) × 360(L) × 345(H) mm. The sample was suspended under a fixed iron frame, and the bottom of the sample was immersed in the fluid to about 3 mm. To reduce the influence of water evaporation and water droplets seeping from the sample surface on the experimental results, we made the following improvements: ① the top of the beaker was

sealed with plastic wrap; ② the sides of the sample were coated with wax. The beaker mass change was recorded by a balance automatically as a function of time. The spontaneous imbibition mass was equal to the mass loss of the beaker. Due to the differences between experimental conditions and actual formation conditions and the representativeness of samples, this experiment has some limitations. Although the limitations of the experiment may lead to a certain deviation between the imbibition behavior of experiments and that of the actual situation, the general law presented by the experimental results is applicable.

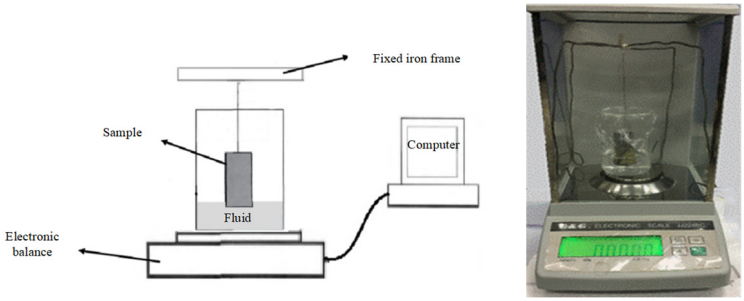

(**a**) (**b**)

Figure 2. The experiment apparatus: (**a**) the experimental device schematic diagram; (**b**) the experimental apparatus.

The flowchart for spontaneous imbibition experimental is shown in Figure 3. The spontaneous imbibition experiments performed in this study can be categorized into three sets. The test procedures and objectives of each set are summarized below. The experiment usually ended when the spontaneous imbibition tended to stabilize. It took one week for high-permeability samples and one month for low-permeability samples.

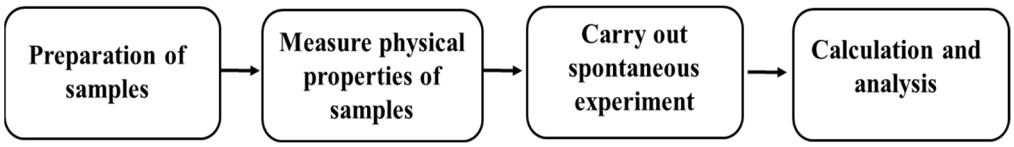

Figure 3. The flowchart for spontaneous imbibition experimental.

(1) Set 1 (investigating the typical characteristics of spontaneous imbibition in shale reservoirs) The objective of this set is to reveal the characteristics of spontaneous imbibition for shale. The test procedure includes the following steps:
   - ① Leave the bottom of the sample immersed into the fluid about 3 mm and measure the mass of the beaker.
   - ② Measure the mass loss of the beaker at a certain time interval.
   - ③ Change the sample and repeat steps ① and ②.

(2) Set 2 (investigating the effect factors on spontaneous imbibition in shale reservoirs) The objective of this experiment is to investigate the effect factors on spontaneous imbibition in shale reservoirs. The test procedure includes the following steps:
   - ① Cut shale into columnar samples with fixed area (19.6 cm^2) and length (50 mm), and cuboid samples with different areas (ranging from 4.84 to 8.20 cm^2) but the same height (50 mm) and measure the physical parameters of samples, such as length, diameter, porosity, permeability, mass and so on.
   - ② Leave the bottom of the sample immersed in the fluid to about 3 mm and measure the mass loss of the beaker at a certain time interval.
   - ③ Change the contact area, porosity, initial water saturation, and fluid type and repeat step ②.

(3) Set 3 (investigating the influence of spontaneous imbibition on porosity and permeability of shale)

The objective of this set is to investigate the influence of spontaneous imbibition on porosity and permeability of shale. The test procedure includes the following steps:

① Measure the dry sample mass, porosity and permeability. The permeability measurement adopts steady axial flow of gas, with a confining pressure of 2.76 MPa and a pore pressure of 0.60 MPa. The porosity measurement adopts Boyle's law double chamber method, with the inlet pressure 1.38 MPa.

② Leave the bottom of the sample immersed into the fluid about 3 mm.

③ Take out the sample after the water imbibed mass reaches a stable level and dry it. Measure the sample mass, porosity and permeability.

④ Repeat the step ② and ③ twice.

2.3. Data Processing

Handy [39] (1960) assumed that the gas-water flow was piston-like displacement during spontaneous imbibition process, and the effects of gas phase pressure gradient of the leading edge and gravity were ignored. Handy established spontaneous imbibition model for gas-water and obtained the imbibed volume expression, as shown in Equation (1).

$$V_{\text{in}} = \sqrt{\frac{2p_{\text{c}}\phi K S_{\text{w}} A_{\text{c}}^2}{\mu_{\text{w}}}}\sqrt{t} \tag{1}$$

where V_{in} is the water imbibed volume, cm^3; p_{c} is the capillary pressure, Pa; ϕ is the porosity, %; K is the permeability, mD; S_{w} is the water saturation of the leading edge, %; A_{c} is the contact surface area, cm^2; μ_{w} is the water viscosity, mPa·s; t is the spontaneous imbibition time, h.

Dividing both side of Equation (1) by the contact surface area, Equation (2) was obtained:

$$\frac{V_{\text{in}}}{A_{\text{c}}} = A_{\text{f}}\sqrt{t} \tag{2}$$

$$A_{\text{f}} = \sqrt{\frac{2p_{\text{c}}\phi K S_{\text{w}}}{\mu_{\text{w}}}} \tag{3}$$

where A_{f} is the rate of spontaneous imbibition. It is related to shale micro-structure, mineral composition, liquid properties and interaction between shale and liquid. In the $\frac{V_{\text{in}}}{A_{\text{c}}} - \sqrt{t}$ coordinate system, the slop of imbibition curve is the rate of spontaneous imbibition, and it can be used to visualize characterize the magnitude of the spontaneous imbibition rate.

The capacity of shale spontaneous imbibition was influenced by many factors. The data of spontaneous imbibition experiment can be normalized to analysis the effects of different factors on shale spontaneous imbibition capacity. Olafuyi et al. [40] (2007) introduced the parameter R that is the ratio of imbibed volume to the pore volume of the core to normalize the imbibition data. The spontaneous imbibition capacity can be characterized by the parameter R. The expression of the parameter R is as follows:

$$R = \frac{V_{\text{in}}}{\phi A_{\text{c}} L} = \sqrt{\frac{2p_{\text{c}} K S_{\text{w}}}{\phi \mu_{\text{w}} L^2}}\sqrt{t} \tag{4}$$

3. Experiment Results and Discussion

3.1. Characteristics of Spontaneous Imbibition for Shale

To reveal the characteristics of spontaneous imbibition, four shale samples were used for experiment. The test fluid was 5% KCl. The physical parameters of samples are listed in Table 2. The mass of spontaneous imbibition was converted to water imbibed volume per unit area using the density of the fluid and Equation (2), and the experiment result is shown in Figure 4. Figure 4 reflects that the curves of spontaneous imbibition have the same trend and the process of the spontaneous imbibition can be divided to 3 stages: the rapid imbibition stage, transitional stage and stable stage.

Table 2. The physical parameters of samples 1–4.

Sample Number	Length (mm)	Diameter (mm)	Porosity (%)	Permeability (mD)
1	50	25	4.34	0.96091
2	50	25	3.80	0.23449
3	50	25	3.68	0.01581
4	50	25	3.11	0.00801

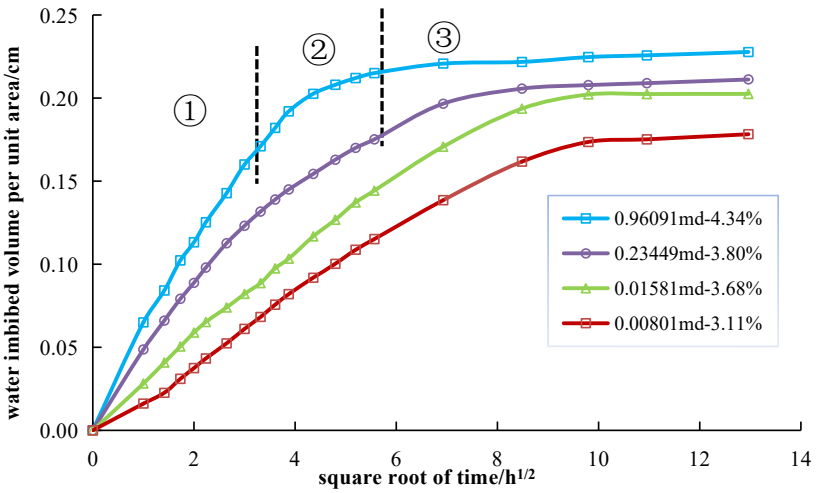

Figure 4. The characteristic curve of the water imbibed volume per unit area over the square root of time. ① is rapid imbibition stage; ② is transitional stage; ③ is stable stage.

① rapid imbibition stage: with the increase of the time, the water imbibed volume increases rapidly. The slope of the curve is equal to the spontaneous imbibition rate.

② transitional stage: with the increase of the time, the slope of the curve gradually decreases to 0. In this stage, the rate of spontaneous imbibition decreases with time. This stage is affected by the permeability. The higher the permeability, the more obvious transitional stage. In Figure 4, the green and red curves correspond to samples with lower permeability (0.01581 and 0.00801 mD, respectively), so the transition stage is not distinct compared with the curves of sample 1 and 2.

③ stable stage: the water imbibed volume varies little, and the slope of the curve is 0. The location of the curve in stable stage represent the spontaneous imbibition capacity per unit area of shale. The higher the location of the curve in stable stage is, the stronger the spontaneous imbibition capacity per unit area of shale will be.

3.2. Sensitivity Analysis

The spontaneous imbibition in shale are affected by the bedding, contact area, porosity, initial water saturation, and fluid type. To study the influence of these factors on sponta-

neous imbibition in shale reservoirs, experiments were carried out according to the test procedure in Section 2.2, and if not specified, the test fluid was 5% KCl. The results are as follows:

(1) The effect of the bedding on spontaneous imbibition

Drill shale cores with parallel and vertical bedding directions at the same location in the 8th and 1st layers of the Longmaxi Formation, respectively. To study the effect of the bedding on spontaneous imbibition, the spontaneous imbibition experiments were carried out by using the columnar shale samples with the same bottom area, length, but different bedding development. The physical parameters of samples were listed in Table 3. The 8th layer of Longmaxi Formation has well-developed bedding and strong heterogeneity in permeability, while the development of bedding in 1th layer of Longmaxi Formation is poor, with low permeability.

Table 3. The physical parameters of samples 5–8.

Sample Number	Length (mm)	Diameter (mm)	Permeability		Layer
			Value(mD)	Method	
5	50	25	0.00402 (vertical bedding Direction)	Boyle's law double chamber method	8th layer
6	50	25	0.10843 (parallel bedding direction)		8th layer
7	50	25	0.00356 (vertical bedding Direction)		1th layer
8	50	25	0.00452 (parallel bedding direction)		1th layer

In order to reflect the influence of bedding on the rate of spontaneous imbibition, the imbibed mass was converted to imbibed volume per unit area using the density of the fluid and Equation (2), and the sensitivity curves were drawn, as shown in Figure 5. Compared samples 5 and 6, the imbibition rate in parallel bedding direction is significantly higher than that in the vertical bedding direction, as shown in Figure 5a. However, compared samples 7 and 8, the imbibition rate in the parallel bedding direction is also greater than that in the vertical bedding direction, but the difference in the two directions is not significant compared with Figure 5a, as shown in Figure 5b. Samples 5 and 6 were drilled from 8th layer of the Longmaxi Formation with well developed bedding, while samples 7 and 8 were drilled from the 1st layer of the Longmaxi Formation with poor development bedding. The elastic modulus and Poisson's ratio in vertical bedding direction are smaller than those in the parallel bedding direction [41]. This often leads to the formation of weak structural planes along the bedding direction. During the imbibition process, under the influence of hydration, microfractures can easily initiate along the parallel bedding direction, which forms an advantageous channel for imbibition. This results result in the imbibition rate of sample 6 being much greater than that of sample 5. For samples 7 and 8, the bedding development is poor, which mainly results in matrix shear failure during the imbibition process. The infiltration exhibits isotropic phenomenon, so the imbibition rate is relatively close. Besides, compared imbibition rate between samples 5 and 7, the imbibition rate is quite different due to the influence of bedding, as shown in Figure 5c. The bedding of sample 5 is more developed than that of sample 7, so its imbibition rate is greater than that of sample 7.

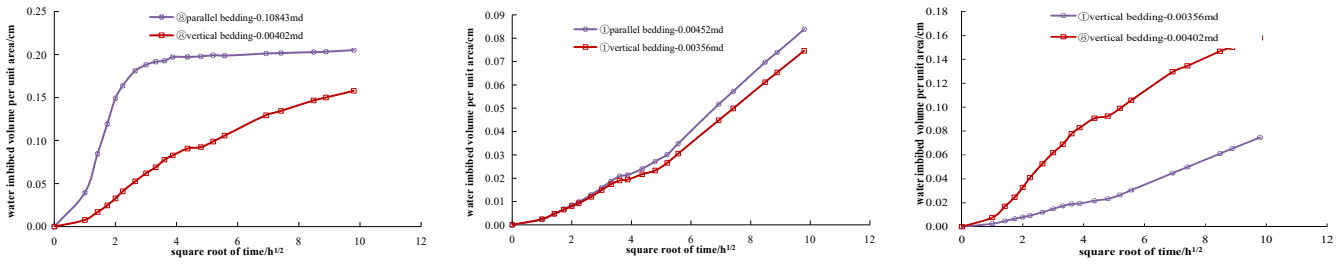

(**a**) (**b**) (**c**)

Figure 5. Comparison of shale spontaneous imbibition in parallel and vertical bedding directions: (**a**) Comparison of shale spontaneous imbibition between sample 5 and 6; (**b**) Comparison of shale spontaneous imbibition between sample 7 and 8; (**c**) Comparison of shale spontaneous imbibition between sample 5 and 7.

In summary, bedding affects shale imbibition rate, which is in consistence with experimental data [42], and the imbibition rate in the parallel bedding direction is greater than that in the vertical bedding direction; the more developed the bedding, the greater the difference in imbibition rates. The finding can be applied to shale with significantly different bedding structures and provides guidance for preventing well wall collapse in bedding developed area during drilling. In the bedding development area, the imbibition speed is fast, which is tend to destroy the stability of borehole walls. Thus, it is necessary to optimize fracturing fluids and add inhibitors to prevent wall collapse.

(2) The effect of contact area on spontaneous imbibition

To study the effect of contact area on spontaneous imbibition, the spontaneous imbibition experiments were carried out by using the cuboid shale samples with the same height, but different bottom area. The physical parameters of samples were listed in Table 4. In order to reflect the influence of contact area on the capacity of spontaneous imbibition, the imbibed mass was converted to imbibed volume using the density of the fluid, and the sensitivity curves were draw, as shown in Figure 6. Figure 6 reflects the capacity of spontaneous imbibition for shale influenced by different areas of water imbibition. The maximum water absorption of the sample with the area of 8.20 cm^2 was 0.96 mL, but the maximum water absorption of the sample with the area of 4.84 cm^2 was 0.65 mL. It is found that the larger contact area is, the greater the capacity of spontaneous imbibition for shale will be. Based on the imbibition results, the analysis shows that when the porosity and the height of samples are the same, the larger contact area is, the larger the pore volume will be, and the more water absorption will be.

Table 4. The physical parameters of samples 9–11.

Sample Number	Height (mm)	Area (cm^2)	Porosity (%)	Permeability (mD)
9	50	8.20	2.33	0.03271
10	50	5.77	2.93	0.03953
11	50	4.84	2.74	0.03597

This finding can be applied to high-pressure, high-temperature conditions typical of deeper reservoirs. Based on this finding, we may understand why the shale reservoir with a better fracturing effect has a lower flowback rate [43,44]. For example, Baima area and Jiaoshiba area are located in Fuling Gas field. Baima area with flowback rate of 16.5% is a deep high-pressure shale gas field, while Jiaoshiba area with flowback rate of 7.3% is a normal pressure shale gas field. Compared with Baima area, Jiaoshiba area has a more complex fracture network after fracturing, and its contact area is larger than that of Baima

area. According to the research results, the imbibition volume of Jiaoshiba area is larger than that of Baima area, which well explains the reason why the flowback rate of fracturing fluids in Jiaoshiba area is lower than that of Baima area.

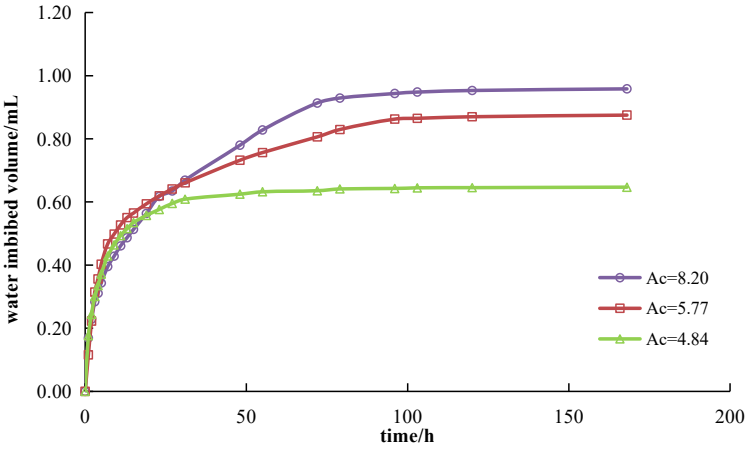

Figure 6. The curve of spontaneous imbibition controlled by different contact area.

(3) The effect of the porosity on spontaneous imbibition

To study the effect of the porosity on spontaneous imbibition, the spontaneous imbibition experiments were carried out by using the columnar shale samples with the same bottom area, length, but different porosity. The physical parameters of samples were listed in Table 5. In order to reflect the influence of the porosity on the capacity of spontaneous imbibition, the imbibed mass was converted to imbibed volume using the density of the fluid, and the sensitivity curves were draw, as shown in Figure 7. Figure 7 reflects the capacity of spontaneous imbibition for shale influenced by the different porosity. The maximum water absorption of the sample with the porosity of 4.51% was 0.62 mL, but the maximum water absorption of the sample with the porosity of 3.74% was 0.55 mL. It is found that the larger the porosity is, the greater the capacity of spontaneous imbibition for shale will be. Based on the imbibition results, the analysis shows that when the volume of samples are the same, the larger the porosity is, the larger the pore volume will be, and the more water absorption will be.

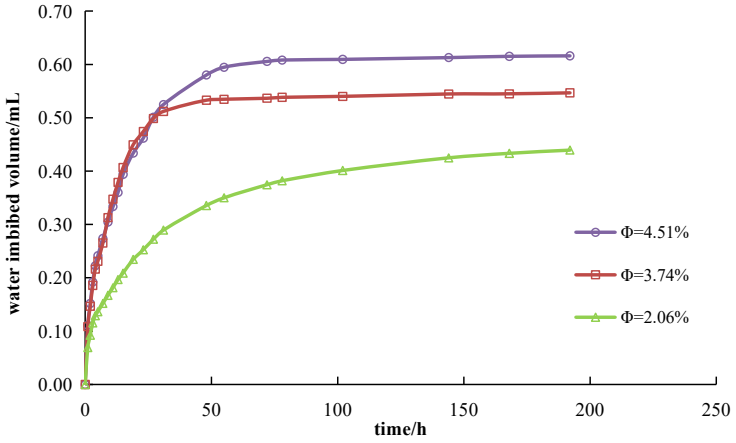

Figure 7. The curve of spontaneous imbibition controlled by different porosities.

Table 5. The physical parameters of samples 12–14.

Sample Number	Length (mm)	Diameter (mm)	Porosity (%)	Permeability (mD)
12	50	25	3.74	0.04253
13	50	25	4.51	0.04397
14	50	25	2.06	0.04017

(4) The effect of the initial water saturation on spontaneous imbibition

To study the effect of the initial saturation on spontaneous imbibition, the spontaneous imbibition experiments were carried out by using columnar shale samples with the same bottom area and length but different initial water saturation. The physical parameters of samples are listed in Table 6. The bedding fractures of the three samples are well developed, so their permeability is relatively high. In order to reflect the influence of the initial water saturation on the capacity of spontaneous imbibition, the imbibed mass was converted to water imbibed volume per unit of pore volume using the density of the fluid and Equation (4), and the sensitivity curves were drawn, as shown in Figure 8. Figure 8 reflects the capacity for spontaneous imbibition for shale influenced by the different initial water saturation. The maximum water imbibed volume per unit pore volume of the sample with a 47.3% initial water saturation was 54.2%, that of the sample with a 35.0% initial water saturation was 67.3%, and that of the sample with a 26.2% initial water saturation was 112.3%. It was found that the higher the initial water saturation is, the less the capacity of spontaneous imbibition will be. Based on the imbibition results, the analysis shows that the higher the initial water saturation is, the smaller the pore volume occupied by the gas per unit pore volume will be and the smaller the water absorption volume per unit pore volume will be. The reason why the maximum water imbibed volume per unit pore volume of the sample with a 26.2% water saturation is more than 100% is that the porosity of the sample was increased resulted from the spontaneous imbibition.

Table 6. The physical parameters of samples 15–17.

Sample Number	Length (mm)	Diameter (mm)	Porosity (%)	Permeability (mD)	Saturation (%)
15	50	25	2.92	1.16313	47.3
16	50	25	2.56	1.18321	35.0
17	50	25	2.60	1.35217	26.2

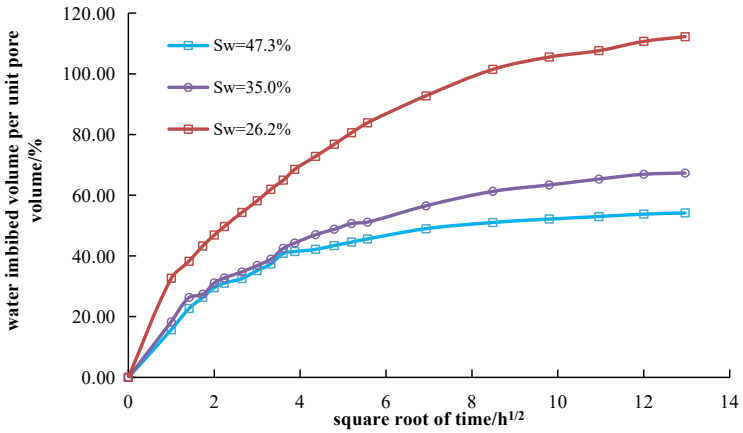

Figure 8. The curve of spontaneous imbibition controlled by different initial saturation.

(5) The effect of the fluid type on spontaneous imbibition

To study the effect of the fluid type on the spontaneous imbibition capacity of shale, the spontaneous imbibition experiments were carried out by using distilled water, 5% KCl solution and kerosene. The physical parameters of samples were listed in Table 7. In order to reflect the influence of the fluid type on the spontaneous imbibition capacity of shale, the imbibed mass was converted to water imbibed volume per unit pore volume using the density of the fluid and Equation (4), and the sensitivity curves were drawn, as shown in Figure 9. Figure 9 reflects the capacity of spontaneous imbibition for shale influenced by the different fluids. The maximum imbibed volume per unit pore volume of shale in distilled water was 65.7%, that in 5% KCl solution was 56.4%, and that in kerosene was 32.7%. It was found that the spontaneous imbibition capacity of shale in different solutions is as follows: distilled water > 5% KCl solution > kerosene. Based on the imbibition results, the analysis shows that the pores in shale are mainly divided into two types: organic pores and inorganic pores. The imbibition of distilled water and 5% KCl solution into inorganic pores are mainly affected by capillary force and osmotic. The imbibition of kerosene into organic pores is mainly affected by capillary force. The osmotic pressure is related to the salinity difference between the fluid and shale, and the greater the salinity difference is, the greater the osmotic pressure will be. Under the same pore radius, the greater the surface tension is, the greater the capillary force will be. The osmotic pressure of distilled water is bigger than that of 5% KCl solution for the salinity difference between the distilled water, and that of shale is bigger than that between the 5% KCl solution and shale. The surface tension of distilled water is the largest, while the surface tension of the kerosene is the least. Therefore, under the same pore radius condition, the capillary force of distilled water is the largest, and that of kerosene is the least. Considering the influence of the capillary force and osmotic pressure, the imbibition capacity of shale in each solution is as follows: distilled water > 5% KCl solution > kerosene.

Table 7. The physical parameters of the sample 18–20.

Sample Number	Length (mm)	Diameter (mm)	Porosity (%)	Permeability (mD)	Fluid
18	50	25	4.10	0.04171	Distilled water
19	50	25	4.30	0.04244	5% KCl solution
20	50	25	3.97	0.03743	kerosene

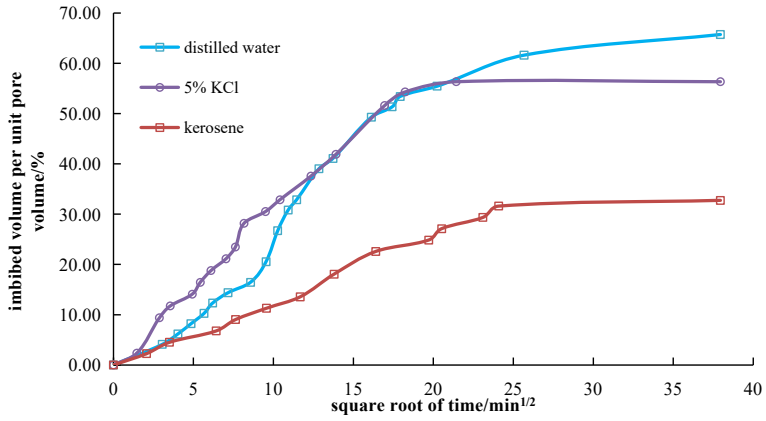

Figure 9. The curve of spontaneous imbibition controlled by different fluids.

3.3. Spontaneous Imbibition Impact on Porosity and Permeability of Shale

To study the effect of spontaneous imbibition on porosity and permeability of shale, the spontaneous imbibition experiments were carried out using two typical columnar shale

samples. One was a matrix sample (No. 21) with an initial permeability of 0.021 mD and porosity of 1.12%; the other was a fractured sample (No. 22) with an initial permeability of 0.083 mD and a porosity of 3.01%. The physical parameters of the two samples are listed in Table 8. Both samples were used to imbibe the water three times. After each spontaneous imbibition, the sample was dried for the next imbibition. The porosity of the two samples and imbibed mass after each spontaneous imbibition were measured, as shown in Figure 10. Additionally, the permeability of the two samples after each spontaneous imbibition were measured, as shown in Figure 11.

Table 8. The physical parameters of the samples 21–22.

Sample Number	Length (mm)	Diameter (mm)	Porosity (%)	Permeability (mD)
21	81	25	1.12	0.02112
22	81	25	3.01	0.08300

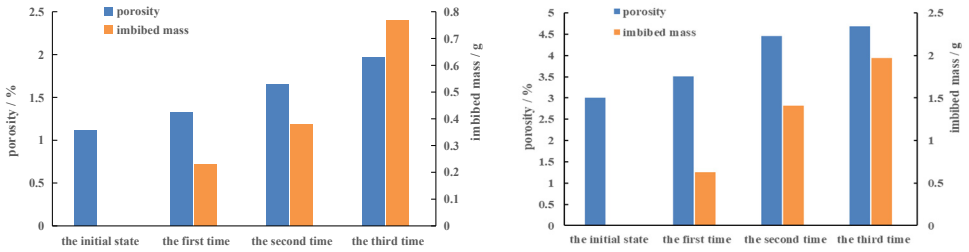

(**a**) (**b**)

Figure 10. The comparison curve of porosity and imbibed mass before and after spontaneous imbibition: (**a**) the comparison curve of matrix sample; (**b**) the comparison curve of fractured sample.

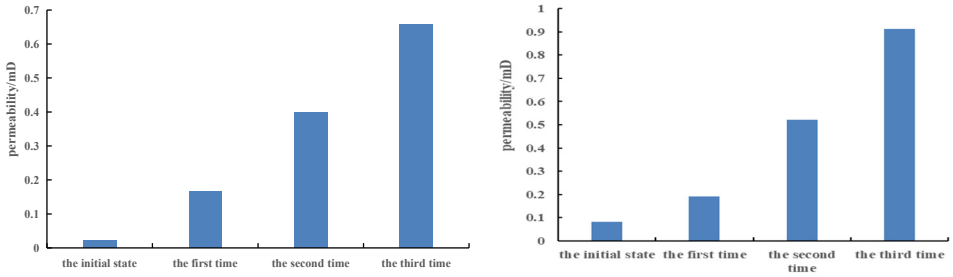

(**a**) (**b**)

Figure 11. The comparison curve of permeability before and after spontaneous imbibition: (**a**) the comparison curve of matrix sample; (**b**) the comparison curve of fractured sample.

The initial porosity and permeability of the matrix sample were 1.12% and 0.021 mD, respectively. After the first imbibition, the porosity increased from 1.12% to 1.33%, the permeability of the matrix sample increased from 0.021 mD to 0.166 mD, and the imbibed mass was 0.23 g. After the second imbibition, the porosity increased from 1.33% to 1.65%, the permeability increased from 0.166 mD to 0.398 mD, and the imbibed mass increased from 0.23 g to 0.38 g. After the third imbibition, the porosity increased from 1.65% to 1.97%, the permeability increased from 0.398 mD to 0.657 mD, and the imbibed mass increased from 0.38 g to 0.77 g.

For the fractured sample, the initial porosity and permeability of the sample were 3.01% and 0.083 mD, respectively. After the first imbibition, the porosity increased from 3.01% to 3.51%, the permeability of the sample increased from 0.083 mD to 0.190 mD, and the imbibed mass was 0.63 g. After the second imbibition, the porosity increased from 3.51% to 4.46%, the permeability increased from 0.190 mD to 0.522 mD, and the imbibed

mass increased from 0.63 g to 1.41 g. After the third imbibition, the porosity increased from 4.46% to 4.69%, the permeability increased from 0.522 mD to 0.912 mD, and the imbibed mass increased from 1.41 g to 1.97 g.

As Figure 12 shows, before the first imbibition, there were no fractures in the matrix sample. After the first imbibition, fractures could be observed in the matrix sample. After the second imbibition, it could be seen that the fractures had expanded significantly. As Figure 13 shows, with the increase of imbibition times, the increase and expansion of fractures in the fractured sample can be observed by naked eye. Under a microscope with a magnification of 6 × 15 and scale of 200 px = 28.00 mm, three fractures can be seen in the top surface of sample 22 after first imbibition, and the average fracture width is 145.97 μm, 195.80 μm, and 259.09 μm, respectively, as shown in Figure 14. After the second imbibition, the average fracture width increased to 296.323 μm, 355.481 μm, and 324.074 μ, as shown in Figure 15. It was found that spontaneous imbibition increases the porosity and permeability of shale, which is consistent with experiment data [35]. Based on the imbibition results, the analysis shows that the water enters the crystal layer of clay mineral and water–rock interaction leads to the destruction of the clay micro-structure and the decrease of the intergranular bonding force, which communicates to the "dead pores" that water cannot enter and increases the effective porosity. Moreover, the permeability increasing is caused by the clay mineral dissolution and microfracture formation and expansion when the water is imbibed into the sample. The results support the idea that the spontaneous imbibition is beneficial to production [33–35] and help us to understand why the shutdown of wells after fracturing can increase gas production [45,46]. The imbibition is beneficial in strengthening the water–rock interaction to generate new fractures and further optimize and transform the reservoir during the shutdown of wells after fracturing. Overall, the long-term effects of spontaneous imbibition on production rates is positive. In the southwestern area of the Jiaoshiba area, we are exploring the use of water flooding to enhance shale gas recovery. We will report the results at the end of the trial.

Figure 12. Comparison of the matrix sample photos before and after spontaneous imbibition: (**a**) matrix sample photo before spontaneous imbibition; (**b**) matrix sample photo after the first time spontaneous imbibition; (**c**) matrix sample photo after the second time spontaneous imbibition.

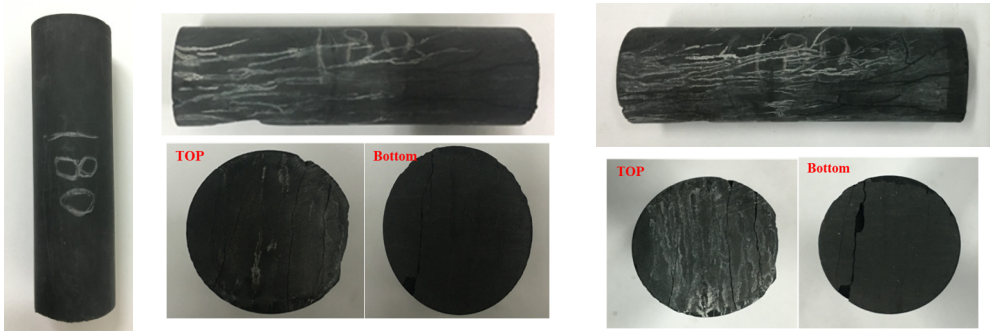

(**a**) (**b**) (**c**)

Figure 13. Comparison of the fractured sample photos before and after spontaneous imbibition: (**a**) fractured sample photo before spontaneous imbibition; (**b**) fractured sample photo after the first time spontaneous imbibition; (**c**) fractured sample photo after the second time spontaneous imbibition.

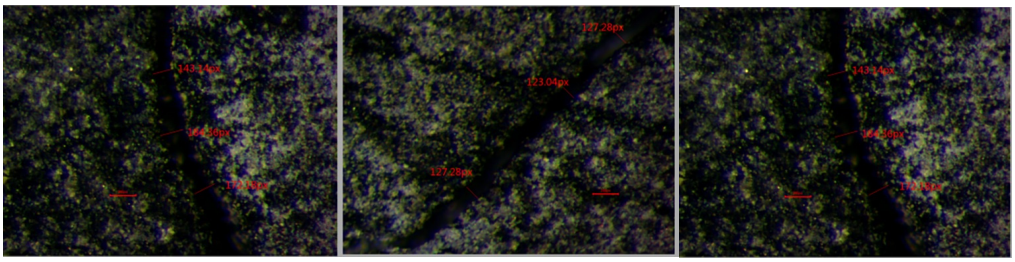

Figure 14. Microscopic view of the top of the fractured sample after the first imbibition (left to right).

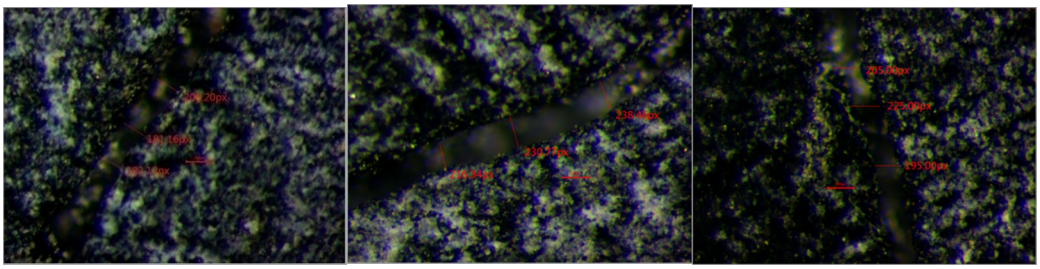

Figure 15. Microscopic view of the top of the fractured sample after the second imbibition (left to right).

4. Conclusions

This paper examined the spontaneous imbibition process in shale, its impact on porosity and permeability, and the effects of bedding, contact area, porosity, initial water saturation, and fluid type on imbibition behavior. The key conclusions drawn from the experimental results are as follows:

(1) The spontaneous imbibition process can be divided into three distinct stages: rapid imbibition, transitional, and stable stages.
(2) Bedding significantly influences the imbibition rate, with the rate being higher in the parallel bedding direction than in the vertical direction. The more developed the bedding, the greater the difference in imbibition rates.
(3) The spontaneous imbibition capacity increases with larger contact area and higher porosity but decreases as initial water saturation rises.
(4) Fluid type affects the imbibition capacity of shale. The imbibition capacity follows this order: distilled water > 5% KCl solution > kerosene.
(5) Spontaneous imbibition enhances both the porosity and permeability of shale.

(6) Future studies can be carried out in the following two directions: ① Considering the influence of confining pressure and temperature, the experimental device will be further improved to simulate the spontaneous imbibition under the formation conditions. ② Integration with computational models for better prediction recovery rate of fracturing fluid in shale gas reservoirs.

Author Contributions: Conceptualization, L.L. and Y.-M.W.; methodology, A.-W.Z. and W.-X.Y.; formal analysis, A.-W.Z.; investigation, Q.Z. and Y.-W.T.; data curation, W.-X.Y.; writing—original draft preparation, L.L. and Y.-M.W.; writing—review and editing, Y.-M.W.; analysis, Y.-M.W. and J.-Q.L.; interpretation, M.C. and S.S. All authors have read and agreed to the published version of the manuscript.

Funding: This research received no external funding.

Data Availability Statement: The original contributions presented in this study are included in the article. Further inquiries can be directed to the corresponding author.

Conflicts of Interest: Authors: Li Liu, Yi-Min Wang, Ai-Wei Zheng, Ji-Qing Li, Qian Zhang, Ya-Wan Tang and Wen-Xin Yang are employed by the Jianghan Oilfield Branch Company. The remaining authors declare that the research was conducted in the absence of any commercial or financial relationships that could be construed as a potential conflict of interest.

References

1. Muther, T.; Qureshi, H.A.; Syed, F.I.; Aziz, H.; Siyal, A.; Dahaghi, A.K.; Negahban, S. Unconventional Hydrocarbon Resources: Geological Statistics, Petrophysical Characterization, and Field Development Strategies. *J. Petrol. Explor. Prod. Technol.* **2022**, *12*, 1463–1488. [CrossRef]
2. Guo, W.; Deng, S.; Sun, Y. Recent Advances on Shale Oil and Gas Exploration and Development Technologies. *Adv. Geo-Energy Res.* **2024**, *11*, 81–87. [CrossRef]
3. Lei, Q.; Xu, Y.; Cai, B.; Guan, B.; Wang, X.; Bi, G.; Li, H.; Li, S.; Ding, B.; Fu, H.; et al. Progress and prospects of horizontal well fracturing technology for shale oil and gas reservoirs. *Pet. Explor. Dev.* **2022**, *49*, 191–199. [CrossRef]
4. Wang, J.L.; Wei, Y.S. Optimizing Managed Pressure-Drawdown Flowback for Shale Gas Well with Complex Fracture Network with Fracture Closure and Two-Phase Flowing. In Proceedings of the International Petroleum Technology Conference, Dhahran, Saudi Arabia, 12–14 February 2024.
5. Yuan, X.L.; Huang, C. Research on back row characteristics of Fuling Shale gas field. *Unconv. Oil Gas* **2017**, *4*, 66–70.
6. Vandecasteele, I.; Rivero, I.M.; Sala, S.; Baranzelli, C.; Barranco, R.; Batelaan, O.; Lavalle, C. Impact of shale gas development on water resources: A case study in northern Poland. *Environ. Manag.* **2015**, *55*, 1285–1299. [CrossRef] [PubMed]
7. Meng, M.; Ge, H.; Ji, W.; Shen, Y.; Su, S. Monitor the process of shale spontaneous imbibition in co-current and counter-current displacing gas by using low field nuclear magnetic resonance method. *J. Nat. Gas Sci. Eng.* **2015**, *25*, 336–345. [CrossRef]
8. Meng, M.; Ge, H.; Shen, Y.; Hu, Q.; Li, L.; Gao, Z.; Tian, T.; Chao, J. The effect of clay-swelling induced cracks on imbibition behavior of marine shale reservoirs. *J. Nat. Gas Sci. Eng.* **2020**, *83*, 103525. [CrossRef]
9. Ezulike, D.O.; Adefidipe, O.A.; Fu, Y.; Dehghanpour, H.; Virues, C.J.; Bearinger, D.; Hawkes, R.V.; Jones, R.S. Flowback fracture closure: A key factor for estimating effective pore-volume. *SPE Reserv. Eval. Eng.* **2016**, *19*, 567–582. [CrossRef]
10. McClure, M. The Potential Effect of Network Complexity on Recovery of Injected Fluid Following Hydraulic Fracturing. In Proceedings of the SPE Unconventional Resources Conference, Woodlands, TX, USA, 1–3 April 2014.
11. Liu, Y.; Leung, J.Y.; Chalaturnyk, R.; Virues, C.J.J. Fracturing Fluid Distribution in Shale Gas Reservoirs Due to Fracture Closure, Proppant Distribution and Gravity Segregation. In Proceedings of the SPE Unconventional Resources Conference, Calgary, AB, Canada, 15–16 February 2017.
12. Parmar, J.; Dehghanpour, H.; Kuru, E. Displacement of water by gas in propped fractures: Combined effects of gravity, surface tension, and wettability. *J. Unconvent. Oil Gas Resour.* **2014**, *5*, 10–21. [CrossRef]
13. Qin, B. Numerical Study of Recovery Mechanisms in Tight Gas Reservoirs. Master's Thesis, University of Oklahoma, Norman, OK, USA, 2007.
14. Dou, L.; Xiao, Y.; Gao, H.; Wang, R.; Liu, C.; Sun, H. The Study of Enhanced Displacement Efficiency in Tight Sandstone from the Combination of Spontaneous and Dynamic Imbibition. *J. Pet. Sci. Eng.* **2021**, *199*, 108327. [CrossRef]
15. Cai, J.; Chen, Y.; Liu, Y.; Li, S.; Sun, C. Capillary Imbibition and Flow of Wetting Liquid in Irregular Capillaries: A 100-Year Review. *Adv. Colloid. InterfaceSci.* **2022**, *304*, 102654. [CrossRef] [PubMed]

16. Yang, R.; Hu, Q.; He, S.; Hao, F.; Sun, M. Wettability and Connectivity of Overmature Shales in the Fuling Gas Field, Sichuan Basin (China). *Bulletin* **2019**, *103*, 653–689. [CrossRef]
17. Wang, G.J.; Zhao, Z.F.; Li, K.; Li, A.; He, B. Spontaneous imbibition laws and the optimal formulation of fracturing fluid during hydraulic fracturing in Ordos Basin. Procedia Eng. *Front. Fluid Mech. Res.* **2015**, *126*, 549–553.
18. Karpyn, Z.T.; Alajmi, A.; Radaelli, F. X-ray CT and hydraulic evidence for a relationship between fracture conductivity and adjacent matrix porosity. *Eng. Geol.* **2009**, *103*, 139–145. [CrossRef]
19. Haqparast, S.; Zeinabady, D.; Clarkson, C.R. Investigating the Effect of Capillary Pressure on DFIT and DFIT-FBA Analysis. In Proceedings of the SPE Canadian Energy Technology Conference and Exhibition, Calgary, AB, Canada, 3 March 2024.
20. Li, C.; Xian, C.; Shen, Y.; Ge, H.; Liu, Y. Partial fractional differential model for gasliquid spontaneous imbibition with special imbibition index: Imbibition behavior and recovery analysis. *J. Pet. Sci. Eng.* **2022**, *209*, 109832. [CrossRef]
21. Andersen, P.Ø.; Ahmed, S. Simulation study of wettability alteration enhanced oil recovery during co-current spontaneous imbibition. *J. Pet. Sci. Eng.* **2021**, *196*, 107954. [CrossRef]
22. Belousov, A.; Lushpeev, V.; Sokolov, A.; Sultanbekov, R.; Yan, T.; Ovchinnikov, E.; Shvets, A.; Bushuev, V.; Islamov, S. Hartmann–Sprenger Energy Separation Effect for the Quasi-Isothermal Pressure Reduction of Natural Gas: Feasibility Analysis and Numerical Simulation. *Energies* **2024**, *17*, 2010. [CrossRef]
23. Bondarenko, A.V.; Islamov, S.R.; Ignatyev, K.V.; Mardashov, D. Laboratory studies of polymer compositions for well-kill under increased fracturing. *Perm J. Pet. Min. Eng.* **2020**, *20*, 37–48. [CrossRef]
24. Khormali, A.; Ahmadi, S.; Kazemzadeh, Y. Inhibition of Barium Sulfate Precipitation During Water Injection into Oil Reservoirs Using Various Scale Inhibitors. *Arab. J. Sci. Eng.* **2023**, *48*, 9383–9399. [CrossRef]
25. Bazin, B.; Peysson, Y.; Lamy, F.; Martin, F.; Aubry, E.; Chapuis, C. In-situ water-blocking measurements and interpretation related to fracturing operations in tight gas reservoirs. *SPE Prod. Oper.* **2010**, *25*, 431–437. [CrossRef]
26. Dutta, R.; Lee, C.; Odumabo, S.; Ye, P.; Walker, S.C.; Karpyn, Z.T.; Ayala, L.F. Quantification of Fracturing Fluid Migration Due to Spontaneous Imbibition in Fractured Tight Formations. In Proceedings of the SPE Americas Unconventional Resources Conference, Pittsburgh, PA, USA, 5–7 June 2012.
27. Neshat, S.S.; Greene, J.T.; Newsham, K.E.; Xie, X.; Keating, J.F. Comprehensive Experimental and Simulation Studies on Capillary Pressure in Uncon-ventional Production and CO_2 Sequestration. In Proceedings of the Annnual Technical Conference and Exhibition, New Orleans, LA, USA, 23–25 September 2024.
28. Dutta, R.; Lee, C.; Odumabo, S.; Ye, P.; Walker, S.C.; Karpyn, Z.; Ayala, L.F. Experimental investigation of fracturing-fluid migration caused by spontaneous imbibition in fractured low-permeability sands. *SPE Reserv. Eval. Eng.* **2014**, *17*, 74–81. [CrossRef]
29. Tian, J.; Chen, Q.; Qin, C.; Kang, Y.; Jia, N.; Xi, Z. Pore-scale systematic study on the disconnection of bulk gas phase during water imbibition using visualized micromodels. *Phys. Fluids* **2022**, *34*, 062015. [CrossRef]
30. Zhang, Y.; Zou, Y.; Zhang, Y.; Wang, L.Y.; Liu, D.Q.; Sun, J.; Ge, H.K.; Zhou, D.S. Experimental Study on Characteristics and Mechanisms of Matrix Pressure Transmission Near the Fracture Surface During Post-Fracturing Shut-In in Tight Oil Reservoirs. *J. Pet. Sci. Eng.* **2022**, *219*, 111133. [CrossRef]
31. Zhou, Z.; Abass, H.; Li, X.; Teklu, T. Experimental investigation of the effect of imbibition on shale permeability during hydraulic fracturing. *J. Nat. Gas Sci. Eng.* **2016**, *29*, 413–430. [CrossRef]
32. Sun, H.; Steven, D.; Cutler, J.; Wood, B.; Wheeler, R.; Qi, Q. A novel nondamaging friction reducer: Development and successful slickwater frac applications. In Proceedings of the SPE Eastern Regional Meeting, Morgantown, WV, USA, 12–14 October 2010.
33. Wang, D.M.; Butler, R.; Liu, H.; Ahmed, S. Flow-rate behavior and imbibition in shale. *SPE Reserv. Eval. Eng.* **2011**, *14*, 485–492. [CrossRef]
34. Morsy, S.; Sheng, J.J. Imbibition Characteristics of the Barnett Shale Formation. In Proceedings of the SPE Unconventional Resources Conference, The Woodlands, TX, USA, 1–3 April 2014.
35. Meng, M.; Ge, H.; Shen, Y.; Li, L.; Chao, J. The effect of clay-swelling induced cracks on shale permeability during liquid imbibition and diffusion. *J. Nat. Gas Sci. Eng.* **2020**, *83*, 103514. [CrossRef]
36. Ma, B.Y.; Yang, S.Y.; Hu, Q.H.; Zhang, T.; Pu, X.G.; Han, W.Z. Integrated core flooding-NMR-imbibition experiments for oil recovery studies from lacustrine shales. In Proceedings of the SEG/AAPG International Meeting for Applied Geoscience & Energy, Houston, TX, USA, 28 August–2 September 2022.
37. Lin, Z.Z.; Hu, Q.H.; Yin, N.; Yang, S.; Liu, H.; Chao, J. Nanopores-to-microfractures flow mechanism and remaining distribution of shale oil during dynamic water spontaneous imbibition studied by NMR. *Geoenergy Sci. Eng.* **2024**, *241*, 213202. [CrossRef]
38. Zhang, Q.; Zeng, H.F.; Li, J.X. Imbibition micro-porosity of shale. *Inn. Mong. Petrochem. Ind.* **2019**, *45*, 80–85.
39. Handy, L.L. Determination of effective capillary pressures for porous media from imbibition data. *Soc. Pet. Eng.* **1960**, *219*, 75–80. [CrossRef]
40. Olafuyi, O.; Cinar, Y.; Knackstedt, M.; Pinczewski, W.V. Spontaneous Imbibition in Small Core. In Proceedings of the 2007 SPE Asia Pacific Oil and Gas Conference and Exhibition, Jakarta, Indonesia, 30 October–1 November 2007.

41. Moseley, M.E.; Mintorovitch, J.; Cohen, Y.; Asgari, H.S.; Derugin, N.; Norman, D.; Kucharczyk, J. Early Detection of Ischemic Injury: Comparison of Spectroscopy, Magnetic Susceptibility-Weighted MRI in Cats. In *Brain Edema VIII*; Springer: Vienna, Austria, 1990; pp. 207–209.
42. Makhanov, K.; Habibi, A.; Dehghanpour, H.; Kuru, E. Liquid intake of gas shales: A workflow to estimate water loss during shut-in periods after fracturing operations. *J. Unconv. Oil Gas Resour.* **2014**, *7*, 22–32. [CrossRef]
43. Si, Z.M.; Li, A.F.; Guo, H.X.; Zhang, H.; Fu, S. Experimental study on the influencing factors of fracturing fluid flowback rate in tight reservoir. *Pet. Geol. Recovery Effic.* **2017**, *24*, 122–126.
44. Zou, S.L.; Chu, X.D. On relationship between shale gas well flowback and production rate. *J. Jianghan Pet. Univ. Staff. Work.* **2018**, *31*, 44–47.
45. Cheng, Q.Y.; You, L.J.; Kang, Y.L.; Zhou, Y.; Xu, J.M. Effect of oxidative dissolution on water spontaneous imbibition in shale gas reservoirs. *Pet. Geol. Recovery Effic.* **2020**, *27*, 94–103.
46. Li, C.L.; Mao, W.Y.; Wu, T.X.; Zhu, S.Y. A study on mechanism of oil displacement by imbibition. *Xinjiang Pet. Geol.* **2019**, *40*, 687–694.

Disclaimer/Publisher's Note: The statements, opinions and data contained in all publications are solely those of the individual author(s) and contributor(s) and not of MDPI and/or the editor(s). MDPI and/or the editor(s) disclaim responsibility for any injury to people or property resulting from any ideas, methods, instructions or products referred to in the content.